



Journal of Advanced Research in Applied Mechanics

Journal homepage:
https://semarakilmu.com.my/journals/index.php/appl_mech/index
ISSN: 2289-7895



Crosslink Density and Toluene Sorption of Tin Dioxide Reinforced Deproteinized Natural Rubber Nanocomposites

Choy Jun Hong¹, Noraiham Mohamad^{1,*}, Hairul Effendy Ab Maulod², Jeefferie Abd Razak¹, Toibah Abd Rahim¹, Mohd Sharin Ghani³, Nor Hidayah Rahim³, Soh Tiak Chuan⁴, Dewi Suriyani Che Halin⁴, Mohammed Iqbal Shueb⁵

¹ Fakulti Kejuruteraan Pembuatan, Universiti Teknikal Malaysia Melaka, Hang Tuah Jaya, 76100, Durian Tunggal, Melaka, Malaysia

² Fakulti Teknologi Kejuruteraan Mekanikal & Pembuatan, Universiti Teknikal Malaysia Melaka, Hang Tuah Jaya, 76100, Durian Tunggal, Melaka, Malaysia

³ Fakulti Kejuruteraan Elektrik, Universiti Teknikal Malaysia Melaka, Hang Tuah Jaya, 76100 Durian Tunggal, Melaka, Malaysia

⁴ Rubber Leisure Products Sdn. Bhd., Kawasan Perindustrian Serkam, Daerah Jasin, 77300 Melaka, Malaysia

⁵ Radiation Processing Technology Division, Malaysian Nuclear Agency, Selangor, Malaysia

ARTICLE INFO

Article history:

Received 17 July 2023

Received in revised form 19 September 2023

Accepted 5 October 2023

Available online 13 November 2023

Keywords:

Natural rubber nanocomposites; Tin Dioxide; crosslink density; swell behavior; Toluene Sorption

ABSTRACT

Nowadays, the industry is looking for polymer-based electrical insulators made of greener materials that are more environmentally friendly than existing insulators. In this study, green material of deproteinized natural rubber (DPNR) nanocomposites reinforced with tin dioxide (SnO₂) nanoparticle loadings of 0%, 0.5%, 1%, 3%, and 7% wt% were prepared using melt compounding and vulcanized through sulfur curing. Mechanical properties of DPNR/SnO₂ nanocomposites were evaluated using the tensile test per ASTM D412. The swelling measurement testing was carried out in toluene as a solvent to measure the toluene uptake, swelling rate, sorption coefficient, diffusion coefficient, and permeability coefficient of the DPNR/SnO₂ nanocomposites. The XRD, FTIR, SEM and OM analyses support the results. The nanocomposites' crosslink behavior varied with the variation of SnO₂ nanoparticles in the nanocomposite. The tensile strength of more than 25 MPa was observed at the crosslink density of 1.101 to 1.270 x 10⁻⁴ mol/cm³. Therefore, this research proved the efficient range of the DPNR/SnO₂ nanocomposites, corresponding with 1 to 3 wt% of tin dioxide filler loadings in the DPNR matrix. The findings of this study would bring benefits to the electrical industry with the development of green materials for electrical insulation.

1. Introduction

In recent decades, polymer nanocomposites have gained increasing importance due to their ability to achieve desirable properties. These nanocomposites enable the development of materials with superior properties compared to their individual constituents, opening up new application possibilities that were not achievable with the individual polymers in the blend. Some desired

* Corresponding author.

E-mail address: noraiham@utem.edu.my

<https://doi.org/10.37934/aram.111.1.103119>

property improvements offered by polymer nanocomposites include enhanced tensile strength, impact strength, heat distortion temperature, flame retardancy, permeability characteristics, and electrical properties. Several factors, including the nature of the polymer, blend composition, and interfacial adhesion, influence the physical properties of polymeric materials. Polymer nanocomposites are composites where fillers in the nanometer size range are dispersed within polymers at various weight percentages (wt%). Typically, the fillers used in the matrix are kept minimal, often below 10 wt%. This contrasts traditional composites or polymer microcomposites, where microfillers constitute as high as 50% of the total material weight [1].

Tin dioxide (SnO_2) in the rutile structure is an n-type environmentally friendly semiconductor with a bandgap energy of 3.6 eV [2]. Nanocrystalline SnO_2 exhibits exceptional optical and electrical properties due to its high surface-to-volume ratio and quantum confinement effects. The nanoparticles find applications in photocatalysis, optoelectronics, and spintronics devices [3]. SnO_2 nanoparticles dispersed in a polyethylene oxide (PEO) matrix have been investigated to prepare high-performance nanocomposite solid polymer electrolytes (NSPEs). SnO_2 is also used in transparent organic resistive memory devices, gas sensors, solar cell electrodes, electrochromic windows, and energy storage/converter electrolytes [4]. Blending polymers and incorporating fillers into natural rubber (NR) improves its mechanical properties and electrical insulation characteristics. However, most studies have focused on synthetic rubbers, such as silicone rubber and styrene-butadiene rubber, with limited research on NR's electrical properties.

The presence of solvents in polymers or polymer blends is of significant importance, as most polymers tend to exhibit a reduction in properties when exposed to solvents [5]. Therefore, polymers intended for commercial applications must possess chemical resistance and maintain their mechanical strength and dimensional stability when in contact with solvents. This highlights the transport phenomena's crucial role in various industrial and engineering applications involving polymers. The study of diffusion, sorption, and permeation in composite structures provides valuable means for additional characterization of polymeric materials.

When a crosslinked polymer network comes into contact with a solvent, it absorbs a specific quantity of liquid, which heavily depends on the molecular weight of the liquid and the degree of crosslinking of the polymer. The entry of the solvent into the swollen specimen can result in changes in the weight and size of the polymer [6], potentially leading to distortion or destruction of the sample's microstructure. The interaction between a liquid and rubber can involve liquid absorption, extraction of soluble components, and chemical reactions. The volume change is a useful general measure of a rubber's resistance to a specific liquid. Swelling indicates that the rubber is unsuitable for use in that particular environment.

NR has been extensively studied as an elastomer due to its properties and sustainability. However, no elastomer possesses all the required characteristics for various application areas, so elastomers are commonly reinforced or filled with inorganic materials to enhance their performance. Numerous studies have reported compatible and miscible natural rubber nanocomposites with desirable mechanical properties. Extensive research exists in the literature on diffusion and sorption processes in elastomers and their derivatives, as mentioned in Obasi *et al.*, [5], including studies on natural rubber/epoxidized natural rubber [7], natural rubber/polystyrene [8], nitrile rubber/polypropylene [9], and ethylene-propylene rubber/nylon blends [10]. However, there is still limited reference that solely focuses on solvent sorption effects on deproteinized natural rubber-based nanocomposites. Rattanasom *et al.*, [11] studied the mechanical properties of deproteinized natural rubber compared to synthetic cis-1, 4 polyisoprene for black-filled and unfilled vulcanizates. The role of carbon nanotubes in promoting the properties of carbon black-filled natural rubber/butadiene rubber composites was studied by Gao *et al.*, [12]. Meanwhile, Jiang *et al.*, [13]

focused on preparing high-performance natural rubber/carbon black/molybdenum disulfide nanocomposites and emphasized mechanical properties and abrasion resistance. These studies utilized the equilibrium swelling method to determine the crosslink density using the Flory-Rehner equation.

In a study conducted by Kim *et al.*, [14], the Flory-Rehner equation and the equilibrium swelling theory were employed to calculate rubber specimens' crosslink density and structure. Eq. (1) uses the Flory-Rehner equation to determine the crosslink density (V_{cross}).

$$V_{cross} \left(\frac{mol}{cm^3} \right) = \frac{1}{2M_c} = - \frac{\ln(1 - V_r) + V_r + XV_r^2}{2\rho V_s \left(\sqrt[3]{V_r} - \frac{V_r}{2} \right)} \quad (1)$$

In Eq. (1), the variables are defined as follows: M_c represents the average molecular weight of the rubber between the crosslinks, V_r denotes the volume fraction of the equilibrium swollen rubber, X represents the Flory-Huggins polymer-solvent interaction parameter, V_s corresponds to the molar volume of the solvent used (with a value of 106.27 cm³/mol for toluene), and ρ represents the density of the rubber (measured in g/cm³). Additionally, the values for V_r and X were computed using Eq. (2) and Eq. (3).

$$V_r = \frac{\frac{W_{before} - W_{filler}}{\rho_r}}{\frac{W_{before} - W_{filler}}{\rho_r} + \frac{W_{after} - W_{before}}{\rho_s}} \quad (2)$$

In Eq. (2), the variables are defined as follows: W_{before} (g) represents the initial weight of the rubber sample, W_{after} (g) represents the weight of the rubber sample after swelling, W_{filler} (g) represents the weight of the filler, and ρ_s (g/cm³) represents the density of the solvent.

$$X = \beta + \frac{V_s}{RT} (\sigma_p - \sigma_s)^2 \quad (3)$$

where β is the lattice constant for the polymer-solvent blends (i.e., $\beta = 0.34$), R is the gas constant, T (K) is the absolute temperature (293.15 K), σ_p (MPa^{1/2}) is the solubility parameter of the rubber sample (16.7 MPa^{1/2} for NR), and σ_s (MPa^{1/2}) is the solubility parameter of the solvent (18.0 MPa^{1/2} for toluene). The computed value of X is 0.414.

Moreover, based on Obasi *et al.*, [5], Fickian's second law of diffusion, as illustrated in Eq. (4), may be used to calculate a solvent molecule's diffusion coefficient across a polymer membrane. Where h denotes the blend thickness, θ is the slope of the initial linear component of the Q_t versus \sqrt{t} plot, and Q_∞ is the equilibrium absorption.

$$D = \pi \left(\frac{h\theta}{4Q_\infty} \right)^2 \quad (4)$$

In addition, the toluene sorption statistics were measured in the rubber specimens and reported as the molar percentage absorption (Q_t) of toluene per gram of specimens. The equation stated in Eq. (5) was used to compute Q_t . The molar percentage uptake (Q_t) at each temperature was plotted against the square root of time (\sqrt{t}).

$$Q_t = \frac{\text{Mass of toluene absorbed}}{\frac{\text{Molecular weight of toluene}}{\text{Initial mass of the blend}}} \times 100 \quad (5)$$

To our knowledge, no existing scientific literature reports the analysis of toluene diffusion for DPNR/SnO₂ nanocomposites. Only our previous work on the processability of uncalcined tin dioxide-reinforced deproteinized natural rubber nanocomposites is currently reported [15]. Still, the report does not address the swelling properties of the DPNR/SnO₂ nanocomposites. Meanwhile, in this current work, we focus on investigating the diffusion of toluene, an aromatic solvent, through the nanocomposites and determining the sorption mechanism. We have also calculated the diffusion, sorption, and permeation coefficients while examining the effects of SnO₂ composition. For our investigation, we have chosen toluene as the solvent commonly used in the rubber industry [13].

2. Materials and Methodology

2.1 Raw Materials and Preparation

The formulation recipes employed in this study are provided in Table 1. The primary materials utilized were deproteinized natural rubber (DPNR) and tin dioxide (SnO₂). The DPNR, with a Mooney viscosity UML (1 + 8) of 60±6 MU at 150°C, was procured from Edutech Supply & Services. The commercial ultrafine nano SnO₂, consisting of >99.9% carbon, was obtained from SAT NANO, China. It possessed a specific surface area of 70 m²/g and a 6.48 g/cm³ bulk density. The SnO₂ was utilized in its non-calcined form at various compositions. The vulcanization agent, activator, primary and secondary accelerators, and anti-degradant employed in the study included sulfur, zinc oxide, stearic acid, N-cyclohexyl-2-benzothiazole sulfonamide (CBS), tetramethyl thiuram disulfide (TMTD), and N-(1,3-dimethyl butyl)-N'-phenyl-p-phenylenediamine (6PPD), respectively. These materials were sourced from Lembaga Getah Malaysia.

Table 1

The formulation for preparation of DPNR nanocomposites

Materials/Chemicals	Loading ^a (phr)
DPNR	100
Sulfur	1.5
Zinc oxide	5.0
Stearic acid	2.0
CBS	1.0
TMTD	0.3
6PPD	2.0
SnO ₂ nanoparticles	0.0, 0.5, 1.0, 3.0, 7.0

^a part per hundred rubbers

The compounding process was carried out according to ASTM D-3192 using a Haake internal mixer. The procedure involved the initial mastication of DPNR, followed by adding compounding chemicals (zinc oxide, stearic acid, and 6PPD) after 0.5 minutes of mixing. SnO₂ was then added at the 1-minute mark. After a 2-minute sweep, the compound was transferred to a two-roll mill machine. Subsequently, sulfur and accelerators (CBS and TMTD) were added and mixed for 3 minutes. The compounds were then dumped and left to condition at room temperature for 24 hours. Compression molding was performed at 160°C and 110 kg/force pressure, with the respective cure times (*t*₉₀). This step aimed to produce nanocomposite sheets with appropriate thickness for subsequent testing and analysis.

2.2 Testing and Characterizations

2.2.1 Swelling measurement testing

Swelling measurement testing was conducted to determine the rate of solvent absorption when the samples were immersed in toluene. The samples used for this testing had a diameter of 23.5 mm and a thickness of 2 mm. Toluene was chosen as the solvent for the experiment. The experiment duration ranged from 1 to 3 days, with measurements taken at specific intervals including 1 hour, 3 hours, 24 hours, and 72 hours. Five samples (refer to Figure 1) were prepared with varying amounts of filler, including 0%, 0.5%, 1%, 3%, and 7% of SnO₂ content (refer to Table 1). Each sample consisted of three specimens. All specimens were weighed before being placed in the petri dish to determine their initial weight. The EK-610i Compact Balance was used to measure the specimen weights throughout the experiment. Subsequently, the specimens were re-weighed to obtain their final weight at 1 hour, 3 hours, 24 hours and 3 days (72 hours). At the end of the 72 hours, all swelling data were recorded, and the specimens were dried.

After the swelling measurement, a drying measurement experiment was conducted. Measuring the drying weight of the samples in this swelling experiment allowed for a comparison between the weight during the swelling phase and the weight during the drying phase (de-swelling). The drying measurement experiment to determine the toluene de-swelling rate allows the solvent in the DPNR/SnO₂ nanocomposites samples, which is to be released from the specimen sample. This experiment was conducted after 3 days (72 hours) of the swelling experiment. The drying measurement experiment was then carried out at room temperature, and data on the weight of the specimen was collected at 0 hours, 1 hour, 3 hours, 1 day (24 hours), 3 days (72 hours), 5 days (120 hours), and 7 days (168 hours).

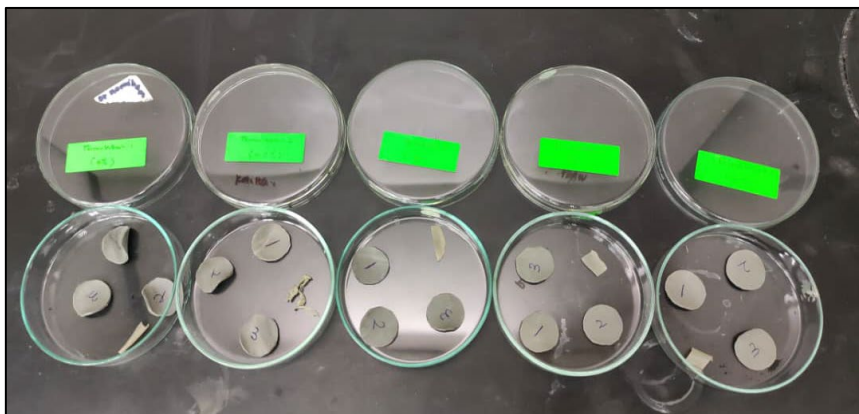


Fig. 1. Swell measurement test carried out in petri dish

Tensile testing was performed on DPNR composites in this study using ASTM D412. A Shimadzu Universal Testing Machine (UTM) was used for the tensile experiment at ambient temperature. The crosshead travel velocity was 500 mm/min. The average value was calculated by repeating five specimens of each sample. In this report, only the tensile strength of the samples is included.

2.2.2 Fourier transform infrared (FTIR) spectroscopy analysis

FTIR spectra were obtained using a JASCO FT/IR 6100 by the KBr pellet technique. The spectrometer was operated at a resolution of 4cm⁻¹ in the scanning range of 450-4000 cm⁻¹ for 50 times scan laser type-II to identify the functional groups of the DPNR/SnO₂ nanocomposites.

2.2.3 X-ray diffraction (XRD) analysis

The compound sheets were characterized by Shimadzu XRD 6000. XRD spectra of the samples were collected over the 2θ range of 1 to 80° using copper $K\alpha$ radiation at a generator voltage 40.0 kV, a generator current of 30.0 mA, wavelength, λ of 1.5418 \AA and a step scan rate of 1.2° in 2θ min^{-1} .

2.2.4 Morphological analyses using optical microscopy and field-emission electron microscopy (FESEM) observation

Optical microscopy was utilized to analyze the molded surface features of the unswollen and swollen samples at $50X$ magnifications. Field-emission electron microscopy (FESEM) Model Gemini SEM 500 from Carl Zeiss was used to identify the swollen fracture surface morphology of DPNR nanocomposites. The morphological inspection on its fracture surface was conducted at $10\ 000x$ magnifications and 2.0kV accelerating voltage.

3. Results & Discussions

3.1 Swelling Rate Measurement

In this swelling measurement experiment, the weight of the sample is measured at 0 hours, 1 hour, 3 hours, 24 hours, and 72 hours. The swelling measurement graph for the weight of toluene uptake by the DPNR/ SnO_2 nanocomposites for 0 , 0.5 , 1.0 , 3.0 and 7.0 wt% filler loadings is shown in Figure 2. The sample with 0.5% filler loadings represents that the sample weighed 0.53 grams at the beginning and rose to 2.12 grams after 72 hours. This data reveals that the sample absorbed the most within the first hour since the weight increased from 0.53 to 1.89 grams.

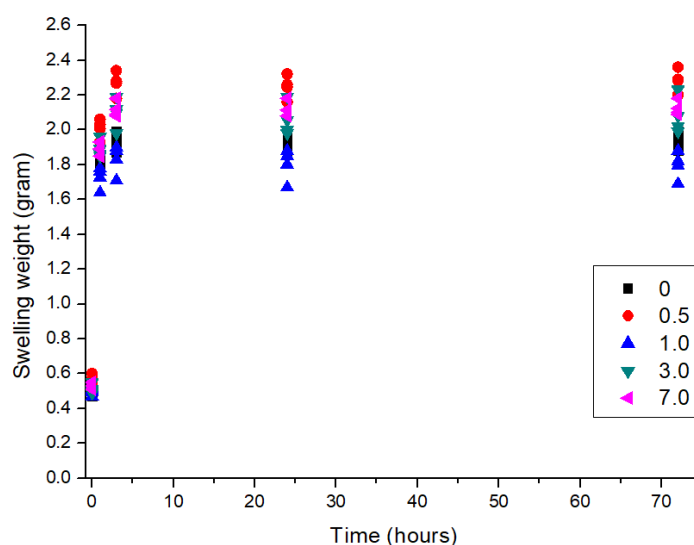


Fig. 2. Swelling weight vs time of DPNR/ SnO_2 nanocomposites with 0 wt%, 0.5 wt%, 1 wt%, 3 wt% and 7 wt% filler loadings

The results indicate that the sample with filler loadings of 0.5 and 7.0 wt% exhibits high swelling ability. In contrast, the sample with filler loadings of 1.0 wt% shows the lowest swelling ability compared to the other specimens. The swelling ability increased in the following order; 1.0 wt%, 3.0 wt%, 7.0 wt% and 0.5 wt% of filler loadings. These findings suggest higher swelling ability is associated

with inhomogeneity and high tin oxide filler loadings. The increased swelling ability can be attributed to voids and agglomerations on the specimen's surface, which may result from poor filler dispersion and distribution levels, excessive SnO₂ and a subsequent decrease in crosslink density. However, it should be noted that the samples with filler loadings of 1.0 to 3.0 wt% may have efficiently formed crosslinks, considering the highest tensile strength observed at 3.0 wt% filler loading and the subsequent decrease at 7.0 wt%.

3.2 De-swelling Rate Measurement

Figure 3 and Table 3 show the de-swelling data of the nanocomposites. The behaviour of toluene release in all samples manifests a three-step process.

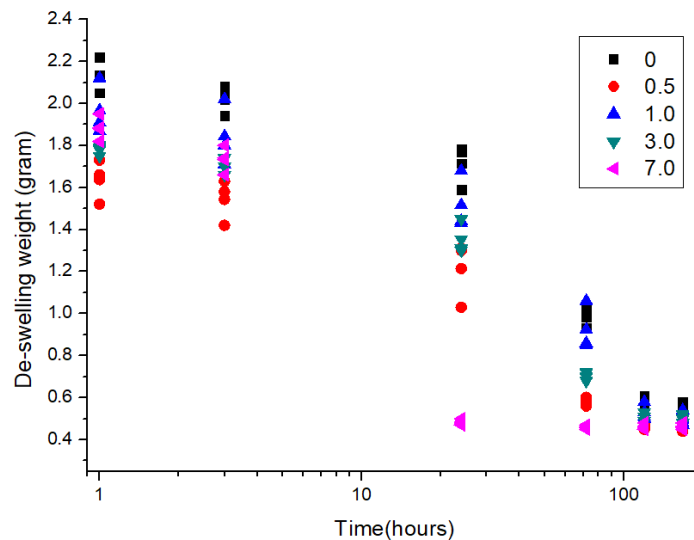


Fig. 3. De-swelling weight vs time for DPNR/SnO₂ nanocomposites with 0 wt%, 0.5 wt%, 1 wt%, 3 wt% and 7 wt% filler loadings

Table 3

Toluene released rate among every DPNR/SnO₂ nanocomposite with 0 wt%, 0.5 wt%, 1.0 wt%, 3.0 wt% and 7.0 wt% filler loadings

Filler Loadings (wt%)	Deswelling rate (g/hrs)			Equation	R-squared
	Step 1	Step 2	Step 3		
0.0	0.09	0.15	0.01	$y = -0.0037x^6 + 0.0853x^5 - 0.7654x^4 + 3.3552x^3 - 7.5525x^2 + 8.0875x - 0.9232$	1.00
0.5	0.08	0.14	0.00	$y = -0.0038x^6 + 0.0845x^5 - 0.7295x^4 + 3.0714x^3 - 6.6286x^2 + 6.7861x - 0.7835$	1.00
1.0	0.14	0.14	0.00	$y = -0.003x^6 + 0.0663x^5 - 0.5502x^4 + 2.1629x^3 - 4.1481x^2 + 3.3487x + 1.2468$	1.00
3.0	0.08	0.13	0.00	$y = -0.0017x^6 + 0.0394x^5 - 0.7295x^4 + 1.4597x^3 - 3.1622x^2 + 3.2204x + 0.8696$	1.00
7.0	0.07	0.18	0.00	$y = -0.0157x^4 + 0.2858x^3 - 1.7275x^2 + 3.5869x - 0.2376$	0.94

It is revealed that the samples with 1.0 wt% tin dioxide filler loadings has the greatest ranking on the toluene released rate. It could be because the least amount of toluene penetrated the nanocomposite network. Conversely, the specimen sample with 7.0 wt% tin dioxide filler loadings has the lowest ranking on the toluene released rate. Table 3 represents the toluene released rate

among all DPNR/SnO₂ nanocomposites with 0 wt%, 0.5 wt%, 1.0 wt%, 3.0 wt%, and 7.0 wt% filler loadings. The results clearly show that the toluene release rate on DPNR/SnO₂ nanocomposites has been divided into three stages: first, second, and third. The results show that all the specimen samples released the solvent dramatically in the first step, the fastest in the second step, and then slowed down in the last step. The last step was when the DPNR/SnO₂ nanocomposites had achieved the equilibrium release rate of the toluene, and the release rate slowed down. The results proved that the suitable filler loadings of tin dioxide in the DPNR matrix would increase the solvent release rate of the sample. The efficient crosslinking that has taken place assists the capability of the material to desorb the amount of the toluene that has penetrated its chain network during swelling. The observations are in line with the micrographs of the sample.

3.3 Molar Percentage Uptake (Q_t) of Toluene per Gram of DPNR/SnO₂ Nanocomposites

Figure 4 depicts the toluene molar proportion absorption (Q_t) per gram versus the square root of time ($t\sqrt{t}$). The adsorption data of toluene into DPNR/SnO₂ nanocomposites with varied levels of filler loading (0 wt%, 0.5 wt%, 1.0 wt%, 3.0 wt%, and 7.0 wt%) is determined and represented as the molar percentage uptake (Q_t) of toluene per gram of DPNR/SnO₂ nanocomposites.

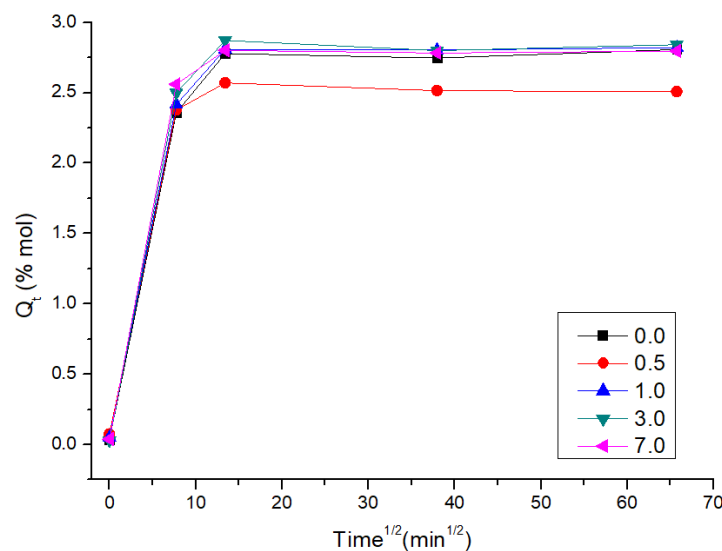


Fig. 4. The variation of equilibrium toluene uptake, Q_t (% mol) of toluene in the DPNR/SnO₂ nanocomposites

Figure 4 shows that the initial increases in the weight of toluene absorbed continued until maximum absorption was attained. At this time, the weight of the absorbed toluene stayed constant, exhibiting equilibrium absorption. The average toluene absorption of the DPNR nanocomposites is between 2.00 to 2.21 %mol. The sample with 1.0 wt% tin dioxide filler loadings has the lowest toluene uptake of only 0.03 %mol at the initial increment stage among the other specimen samples. Meanwhile, the 0.5 wt% sample has the lowest total toluene uptake with a value of 2.51 %mol at 72 hours, reflecting the highest crosslink density. Hayaemasae & Ismail [16] state that the lower the toluene uptake into the reinforcement, the higher the degree of crosslink density.

3.4 Diffusion, Sorption and Permeation of Nanocomposites

Table 4 represents a toluene molecule's diffusion, sorption, and permeation coefficients through DPNR/SnO₂ nanocomposites with different SnO₂ filler loadings. In this study, Fickian's second diffusion rule may be utilized to compute the diffusion coefficient of a solvent molecule via a DPNR/SnO₂ nanocomposites specimen. The diffusion, sorption and permeation coefficients are generally increased by adding SnO₂ nanoparticles into the DPNR matrix. The results demonstrate that the nanocomposite at 7.0 wt% of filler loadings has the highest diffusion, sorption and permeation coefficients compared to the control and other nanocomposite samples. Based on the Swapna *et al.*, [17] study, too high a sorption coefficient may indicate poor rubber-solvent interaction in the presence of filler. It is in agreement with the value observed at 7 wt% filler loadings.

No obvious pattern is observed, but overall, the toluene penetration behavior of the nanocomposites shows an upward tendency compared to the control sample. The increase in filler loadings improves the toluene transport of the nanocomposites. Yet, at the range of filler loadings of 1.0 and 3.0 wt%, nanocomposites' diffusion coefficients and permeation coefficients were slightly decreased. It has been demonstrated that the permeability coefficient of toluene in DPNR/SnO₂ nanocomposites with varying tin dioxide filler loadings is connected to the sorption coefficient (S) for DPNR/SnO₂ nanocomposites. According to Obasi *et al.*, [5], diffusion may control the solvent permeability into the rubber chains. The result indicates that the substance's filler dispersion and crosslink density will influence the diffusion coefficient of a solvent molecule into the DPNR/SnO₂ nanocomposites sample. According to Unnikrishnan & Thomas [18], the crosslinking density mechanism in vulcanized NR is critical for solvent diffusion into the NR matrix.

Table 4
 Sorption properties of DNPR nanocomposites at different filler loadings

Filler Loadings (wt%)	Diffusion Coefficient D (cm ² /min)	Sorption coefficient S (%)	Permeation coefficient P (cm ² /min)
0.0	2.24 x 10 ⁻⁵	5.52 x 10 ⁻²	1.45 x 10 ⁻⁶
0.5	2.63 x 10 ⁻⁵	5.35 x 10 ⁻²	1.20 x 10 ⁻⁶
1.0	2.32 x 10 ⁻⁵	5.78 x 10 ⁻²	1.34 x 10 ⁻⁶
3.0	2.42 x 10 ⁻⁵	6.01 x 10 ⁻²	1.46 x 10 ⁻⁶
7.0	2.65 x 10 ⁻⁵	6.28 x 10 ⁻²	1.67 x 10 ⁻⁶

3.5 Crosslink Characteristics of DPNR/SnO₂ Nanocomposites Calculated Using the Flory–Rehner Equation

Crosslink responses are crucial in enhancing the overall efficiency of rubber. Analyzing rubber's crosslink density and structure yields information that may be used to strengthen the polymer's effectiveness. Figure 5 depicts the correlation between the crosslink density graph with the tensile strength for DPNR/SnO₂ nanocomposites in 0 wt%, 0.5 wt%, 1.0 wt%, 3.0 wt%, and 7.0 wt% of SnO₂ filler loadings. There is no straightforward correlation between crosslink density and nanocomposites' tensile strength (TS). The crosslink density and TS decreased when 0.5 wt% SnO₂ nanoparticles were added to the DPNR matrix. However, the pattern deviated when the amount of filler was larger than 1.0 wt%. It is observed that the highest tensile strength was observed when DPNR was reinforced with 3.0 wt% SnO₂. Crosslink density and TS values associate closely in most samples except for the 7.0 wt filler loadings. It could be due to the role of unpenetrated particles formed in the composites and lessening the absorption of toluene into the rubber chains. This research used the Flory-Rehner equation to determine the crosslink densities and structures of DPNR

composites with different amounts of tin dioxide filler loadings. According to the crosslink density data, the 1.0 wt nanocomposite has the highest crosslink density of $1.27 \times 10^{-4} \text{ mol/cm}^3$. This result was achieved because this specimen sample had the lowest swelling rate, resulting in a high crosslink density. Meanwhile, 0.5 and 7.0 wt% nanocomposites showed lower crosslink density than the control samples.

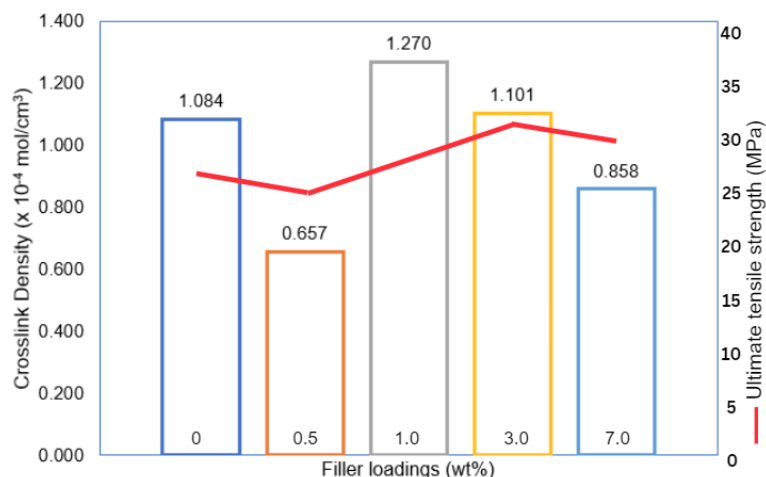


Fig. 5. Correlation between crosslink density to the ultimate tensile strength of the DPNR/SnO₂ nanocomposites

According to Kim *et al.*, [14], since rubber chain immobilization, crosslinked rubber with a large crosslink density may soak up a lesser fraction of solvent molecules, leading to less swelling. The specimen sample with 1.0 wt% tin dioxide filler loadings has the highest crosslink density characteristic compared to the other four nanocomposite samples. Meanwhile, the highest tensile strength was observed in the sample at 3.0 wt% filler loadings, and the 0.5 wt% filler loadings exhibited the lowest. Considering the tensile strength of higher than 25 MPa was obtained by the samples at 1.0 wt% and 3.0 wt%, efficient crosslinking could be obtained at this range where the crosslink density is about 1.10 to 1.27 mol/cm³. The reduction of tensile strength at 7.0 wt% loading could be due to worsened agglomeration effects observed at this rate, as indicated by the SEM micrographs in Figures 8 and 9.

3.6 Structural Characteristics of DPNR/SnO₂ Nanocomposites by X-ray Diffraction (XRD) Analysis

XRD analyses identified differences between non-swelling DPNR/SnO₂ nanocomposites samples regarding structural characteristics [19]. The XRD diffractograms of non-swelling and swelling samples of DPNR/SnO₂ nanocomposites are depicted in Figure 6. Crystalline polymers create sharp peaks in XRD diffractograms, whereas amorphous polymers show broadening peaks [20]. Figure 6(a) shows the XRD spectrum for the non-swelling sample with the filler loadings of 0 wt%, 0.5 wt%, 1.0 wt%, 3.0 wt%, and 7.0 wt%. In the control sample, there is no SnO₂ appearance at θ angles = $\sim 26^\circ$, $\sim 33^\circ$, and $\sim 52^\circ$ due to no SnO₂ nanoparticles being added. Other sharp peaks were from other ingredients, such as zinc oxide. The amorphous polymeric materials structure was shown by the broadening peaks in the 15°-24° range. Three peaks identify the presence of the reaction between DPNR and the SnO₂ filler in the DPNR/SnO₂ nanocomposites at the 2θ angles = $\sim 26^\circ$, $\sim 33^\circ$, and $\sim 52^\circ$. The result in the label area shows that the increase in filler material will affect the increase in peak intensities. The XRD patterns can identify variations in the crystallinity of nanocomposites. The peak of DPNR filled with 0 wt%, 0.5 wt%, 1.0 wt%, 3.0 wt%, and 7.0 wt% of SnO₂ filler loadings showed an

increase in peak intensities, indicating that the DPNR/SnO₂ became more crystalline after doping with the filler material. This peak demonstrated the existence of crystalline structure in DPNR/SnO₂ nanocomposites. According to Abhilash *et al.*, [21], the intensity of the XRD result rises as the filler content increases, indicating that polymer composites have enhanced crystallinity. According to Dang *et al.*, [22], the size and dispersion of nanoparticles formed are impacted by adsorbed ions at the phase interface, which varies with the chemical composition of the molecules.

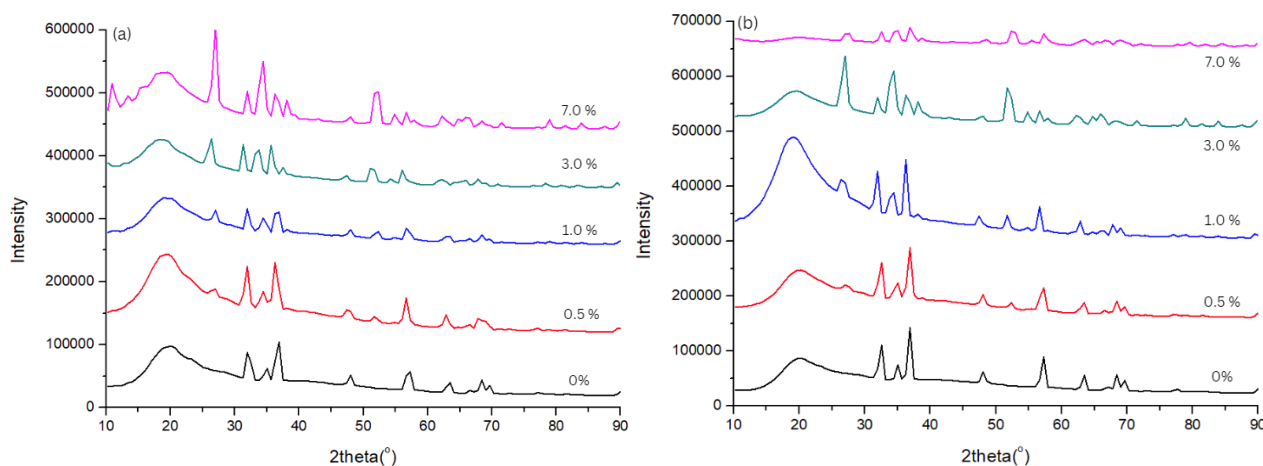


Fig. 6. XRD of DPNR/SnO₂ nanocomposites for (a) non-swelling and (b) swelling samples

Figure 6(b) depicts the XRD combination results for the swelling sample of DPNR/SnO₂ nanocomposites. Interestingly, compared with Figure 6(a), the swollen samples showed polymer regions (amorphous structure) that remained in samples with 0, 0.5 and 1 wt% filler loadings. It manifested by the broadening peaks at 2 θ angles between 15 to 26°. It was reduced in the sample at 3.0 wt% but almost disappeared at 7.0 wt% filler loading. Therefore, the swelling process removed the loosely bound filler particles and the unbound rubber due to the leaching out phenomenon. This observation supported that the good range of SnO₂ filler loadings in the DPNR matrix was between 1 and 3 wt%. It agreed with the observation of the mechanical and swelling properties of the material.

3.7 Fourier Transform Infrared (FTIR) analysis

Fourier Transform Infrared (FTIR) is used to identify the chemical structures of the DPNR/SnO₂ nanocomposites [23] for the non-swelling and swelling samples (refer to Figure 7). In general, the outcome of the FTIR analysis indicates a trivial difference in the effect of filler loadings. Peaks at 399–650 cm⁻¹ wavenumbers correspond to filler loadings of 0.5 wt%, 1 wt%, 3 wt%, and 7 wt%, respectively, and are caused by SnO₂. Following the results, the peak indicates the physical connection and chemical bonding interaction between the DPNR matrix and the nanocomposite's SnO₂ filler loading. According to Abruzzi *et al.*, [24], the peak at ~521 cm⁻¹ corresponds to Sn-OH stretching vibrations, whereas the peak at 660–600 cm⁻¹ relates to Sn-O-Sn stretching vibrations, which are properties of SnO₂. These bands, found at roughly 521 and 620 cm⁻¹, describe the presence of SnO₂ in the composites. All the examined samples showed similar spectra, with the characteristic peaks of SnO₂ being more apparent in the 1 to 7 wt% filler loadings.

FTIR analysis is also employed in this study to identify the chemical structures of the DPNR/SnO₂ nanocomposites for the swollen samples. Kowalczyk & Pitucha [25] state the observed increase in band strength or shift to lower wavenumber values was most likely integrated into the matrix by the changes in the polymer structure. The peak intensity of the FTIR spectra reflects the extent of a

physical connection and chemical bonding interaction between the DPNR matrix and the SnO₂ filler loading. In our case, the swollen samples showed shallower peaks compared to the non-swelling samples (highlighted in red in Figures 7 (a) and (b)). It is notified as the reduction of the functional groups in the samples.

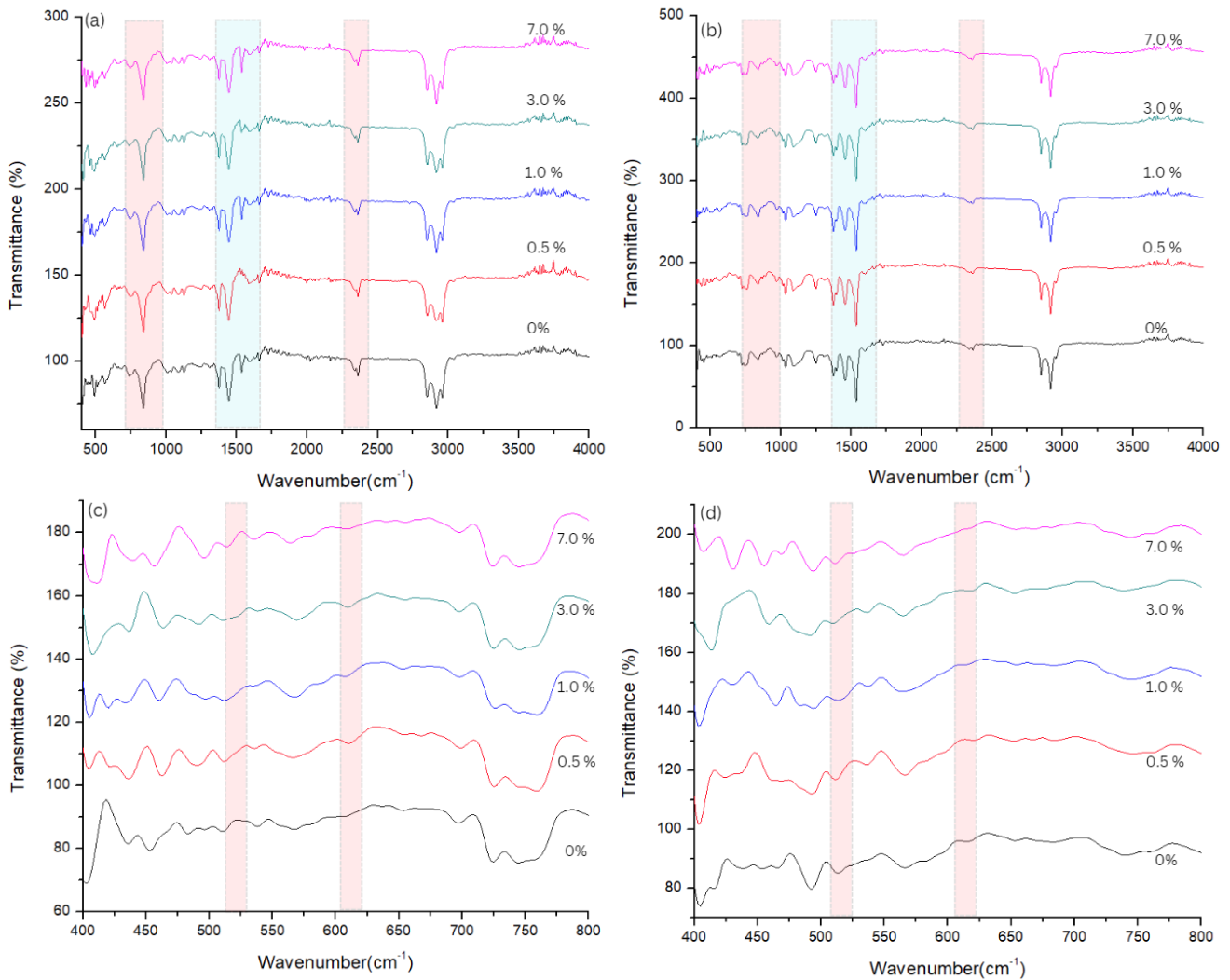


Fig. 7. FTIR spectra of DPNR/SnO₂ nanocomposites for (a) non-swelling sample and (b) swelling sample at 400-4000 cm⁻¹ and (c)-(d) at 400- 800 cm⁻¹

3.8 Physical Surface Criteria through Optical Microscopy (OM) and Scanning Electron Microscopy (SEM) Analyses

The study employs optical microscopy (OM) and SEM analyses to investigate the molded surface of swelling and non-swelling of DPNR/SnO₂ nanocomposites samples with varying filler loadings. The OM analysis in the swelling sample demonstrates that increasing the amount of SnO₂ filler loading influences the growth of agglomeration particles in the specimen sample. The amount of SnO₂ filler used in the specimen sample affects the fillers' distribution and dispersion level, observed by particle agglomerations. Figure 8 represents the OM images at 50X magnifications of DPNR/SnO₂ nanocomposites with 0 wt%, 0.5 wt%, and 3.0 wt% filler loadings for non-swelling and swelling samples. Different contrast reflects the topography gradient of the surface. The dark area represents a rather deeper level compared to brighter areas. A higher portion of the dark area is observed on

the swollen samples, representing the formation of voids due to leached-out components during the swelling process. This outcome may be concluded as the SnO₂ filler material drains away from the specimen sample following the swelling experiment. Besides, it also indicates the extent of agglomerations that occurred in the samples for the effect of filler loadings. Similar to the observations by Spasov *et al.*, [26], agglomeration increases significantly as the filler loading level rises. At too high loading, the pull-out fillers would be drained away from the specimen sample after it undergoes the swelling experiment. The influence of filler loadings on the surface criteria of the nanocomposites is supported by Figure 9. The size of peeled-off debris and the extent of the swollen samples' flakiness at 1000X magnifications increased with the filler loadings.

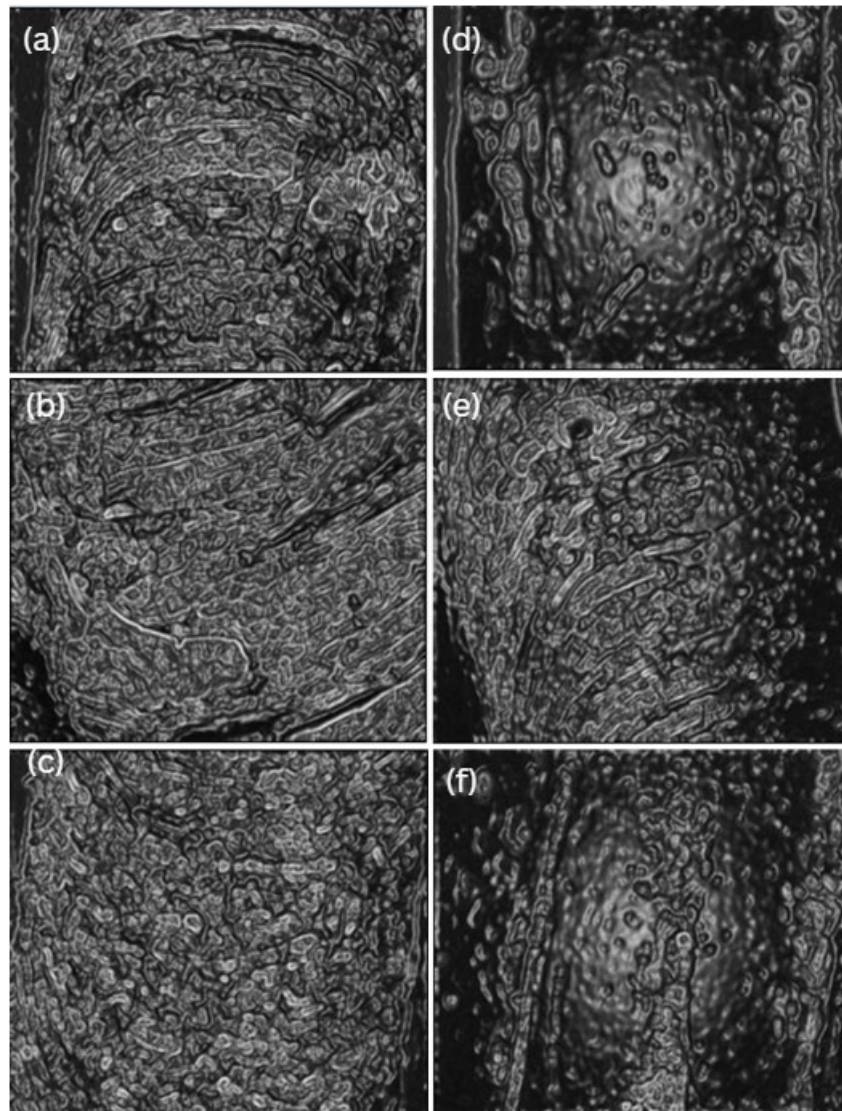


Fig. 8. OM images of DPNR/SnO₂ nanocomposites with 0 wt%, 1.0 wt%, and 7.0 wt% filler loadings for (a-c) non-swelling and (d-f) swelling samples at 50X magnifications

3.9 Tensile fracture surface morphological analysis by Scanning Electron Microscopy (SEM)

The SEM analysis provides information on a specimen's size, shape, composition, crystallography, and other physical and chemical characteristics [27]. Figure 10 depicts the SEM images of DPNR/SnO₂ nanocomposites with 0 wt%, 3.0 wt%, and 7.0 wt% filler loadings for non-swelling and swelling

samples at 1000X magnifications. The morphologies of DPNR composites at different filler loadings showed various features, including dispersed particles, voids, level of dispersion and distribution etc. [28]. In this study, the amount and size of the agglomerates showed a significant increase following the increases in the amount of SnO₂ filler loadings. Voids were found on the fracture surfaces of the specimens tested for DPNR/SnO₂ due to the reinforcements peeling out. Ghazali *et al.*, [29] state that increased filler loading promotes void development due to the effect of agglomeration.

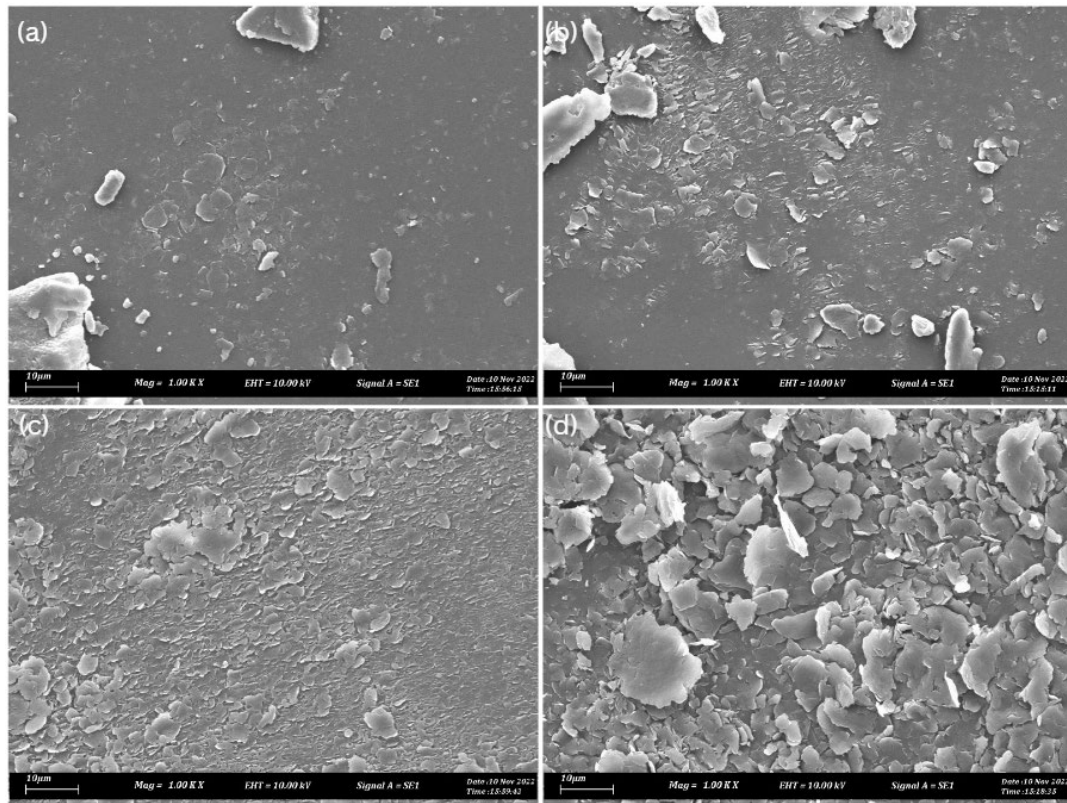


Fig. 9. SEM images of DPNR/SnO₂ nanocomposites with 0 wt%, 0.5 wt%, 1.0 wt% and 7.0 wt% filler loadings for swelling samples at 1000X magnifications

Plastic deformation level could also be observed from the fracture surface of unswollen samples. All samples showed a mixture of ductile (shear yielding) and brittle-like surface failures (smoother surface). Ductile to brittle-like behavior appears to be impacted by the filler loadings [30]. Surface roughness increases at filler loading up to 3.0 wt% and is reduced at 7.0 wt%. In agreement with the observation by Mohamad *et al.*, [31], the observed brittle-like behavior in the DPNR/SnO₂ nanocomposites at higher ratios of fillers to the DPNR matrix may be attributed to the reduced wettability of the matrix on the filler surface. When the ratio of fillers to the DPNR matrix becomes excessively high, it can lead to premature or brittle fractures.

In contrast, the swelling sample of DPNR/SnO₂ nanocomposites differs from the non-swelling sample. The swelling samples appeared to have smoother surfaces with tiny voids compared to unswollen samples. This observation supported the leached-out phenomenon that might be happened to the exposed agglomerated fillers. The nanocomposites at 7.0 wt% filler loadings exhibited the smoothest surface with a higher concentration of voids. It corresponds to particle agglomerates pulled out and leached compared to the samples at 3.0 wt% filler loadings. In the swelling sample at 3.0 wt% filler loadings, there is still obvious shear yielding with rougher surfaces. This nanocomposite failure is caused by better interaction between the DPNR matrix and SnO₂ nanofiller, promoting efficient crosslinking. It is normally observed by low toluene uptake into the

samples due to the formation of crosslink [32]. Thus, non-homogeneous dispersion of SnO₂ at too high filler loading in the DPNR matrix may cause void and agglomeration, negatively impacting mechanical and physical characteristics.

Crosslink responses are crucial in enhancing the overall efficiency of rubber. Analyzing rubber's crosslink density and structure yields information that may be used to strengthen the polymer's effectiveness. Figure 5 depicts the correlation between the crosslink density graph with the tensile strength for DPNR/SnO₂ nanocomposites in 0 wt%, 0.5 wt%, 1.0 wt%, 3.0 wt%, and 7.0 wt% of SnO₂ filler loadings.

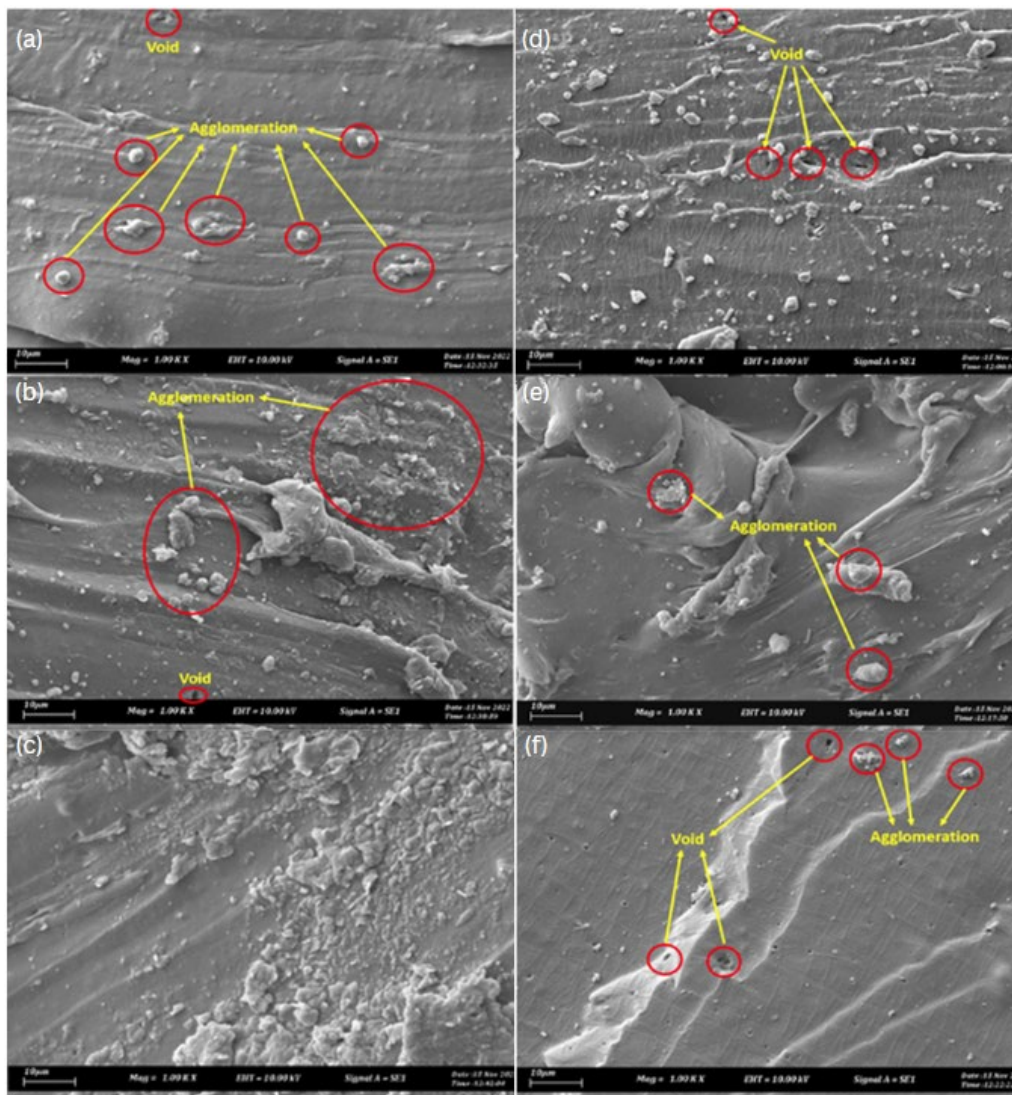


Fig. 10. SEM images of DPNR/SnO₂ nanocomposites with 0 wt%, 3.0 wt%, and 7.0 wt% filler loadings for (a-c) non-swelling and (d-f) swelling samples at 1000X magnifications

4. Conclusions

The DPNR/SnO₂ nanocomposites at 1.0 wt% filler loadings exhibit the highest crosslink density of $1.270 \times 10^{-4} \text{ mol/cm}^3$. Therefore, the efficient crosslink density corresponds to increased mechanical properties. Optimal filler addition quantities range between 1 to 3 wt% of SnO₂, as these formulations demonstrate the highest tensile strength and efficient crosslink density. The effective crosslinking in

the DPNR/SnO₂ nanocomposites results in a reduced swelling rate and improved tensile strength reflected by compositional and structural attributes. Regarding morphological characteristics, the DPNR/SnO₂ nanocomposites with 1.0 and 3.0 wt.% SnO₂ nanoparticles display minimal agglomeration, leading to less leached-out during swelling. Their efficient crosslinks limit the absorption of toluene particles into the composites. Additionally, as the nanocomposites were overloaded with SnO₂ filler at 7.0 wt%, the fracture surface of DPNR/SnO₂ nanocomposites exhibited a more brittle behavior.

Acknowledgement

Special acknowledgement to the Tin Industry (Research and Development) Board, Kementerian Air, Tanah Dan Sumber Asli, Malaysia, for KHAS-TIN/2021/FKP/C00007 grant. The authors would like to thank Universiti Teknikal Malaysia Melaka (UTeM), Rubber Leisure Products Sdn. Bhd. and the Malaysian Nuclear Agency for their facilities and support.

References

- [1] Lau, Kwan Yiew, and M. A. M. Piah. "Polymer nanocomposites in high voltage electrical insulation perspective: a review." *Malaysian Polymer Journal* 6, no. 1 (2011): 58-69.
- [2] Su, Lei, and Yi Huang. "Research on Magnetic Property of Environmental Friendly Material SNO2: MN, S." *E3S Web of Conferences* 237, no. January (2021): 01023. <https://doi.org/10.1051/e3sconf/202123701023>.
- [3] Zulfiqar, Yuliang Yuan, Zahid Iqbal, and Jianguo Lu. "Zn-Doped SnO₂ Nanoparticles: Structural, Optical, Dielectric and Magnetic Properties." *International Journal of Modern Physics B* 31, no. 30 (2017): 1750234. <https://doi.org/10.1142/s0217979217502344>.
- [4] Dhatarwal, Priyanka, Shobhna Choudhary, and R. J. Sengwa. "Significantly Enhanced Dielectric Properties and Chain Segmental Dynamics of PEO/SnO₂ Nanocomposites." *Polymer Bulletin* 78, no. 5 (2020): 2357–73. <https://doi.org/10.1007/s00289-020-03215-2>.
- [5] Obasi, Henry Chinedu, O. Ogbobe, and Isaac O. Igwe. "Diffusion Characteristics of Toluene into Natural Rubber/Linear Low Density Polyethylene Blends." *International Journal of Polymer Science* 2009, no. January (2009): 1–6. <https://doi.org/10.1155/2009/140682>.
- [6] Nair, Kalaprasad Gopalan, and Alain Dufresne. "Crab Shell Chitin Whisker Reinforced Natural Rubber Nanocomposites. 1. Processing and Swelling Behavior." *Biomacromolecules* 4, no. 3 (2003): 657–65. <https://doi.org/10.1021/bm020127b>.
- [7] Johnson, T., and Sabu Thomas. "Natural Rubber/Epoxy Natural Rubber-25 Blends: Morphology, Transport Phenomena and Mechanical Properties." *Journal of Materials Science* 34, no. 13 (1999): 3221–39. <https://doi.org/10.1023/a:1004638024590>.
- [8] Asaletha, R., M. G. Kumaran, and Sabu Thomas. "Transport Behaviour of Aliphatic Hydrocarbons through Dynamically Crosslinked Natural Rubber/Polystyrene Blends." *Polymers & Polymer Composites* 6, no. 6 (1998): 357–71. <https://doi.org/10.1177/147823919800600601>.
- [9] George, Soney C., Gabriël Groeninckx, K. N. Ninan, and Sabu Thomas. "Molecular Transport of Aromatic Hydrocarbons through Nylon-6/Ethylene Propylene Rubber Blends: Relationship between Phase Morphology and Transport Characteristics." *Journal of Polymer Science Part B*, no. January (2000). [https://doi.org/10.1002/1099-0488\(20000815\)38:16](https://doi.org/10.1002/1099-0488(20000815)38:16).
- [10] George, Soney C., K. T. Varughese, and Sabu Thomas. "Molecular Transport of Aromatic Solvents in Isotactic Polypropylene/Acrylonitrile-Co-Butadiene Rubber Blends." *Polymer* 41, no. 2 (2000): 579–94. [https://doi.org/10.1016/s0032-3861\(99\)00208-6](https://doi.org/10.1016/s0032-3861(99)00208-6).
- [11] Rattanasom, Nittaya, U. Thammasiripong, and Krisda Suchiva. "Mechanical Properties of Deproteinized Natural Rubber in Comparison with Synthetic cis-1, 4 Polyisoprene Vulcanizates: Gum and Black-Filled Vulcanizates." *Journal of Applied Polymer Science* 97, no. 3 (2005): 1139–44. <https://doi.org/10.1002/app.21781>.
- [12] Gao, Jiangshan, Yan He, Xinglong Gong, and Jin Xu. "The Role of Carbon Nanotubes in Promoting the Properties of Carbon Black-Filled Natural Rubber/Butadiene Rubber Composites." *Results in Physics* 7, no. January (2017): 4352–58. <https://doi.org/10.1016/j.rinp.2017.09.044>.
- [13] Jiang, Yang, Jin-Yuan Wang, Jian Wu, and Yong Zhang. "Preparation of High-Performance Natural Rubber/Carbon Black/Molybdenum Disulfide Composite by Using the Premixture of Epoxy Natural Rubber and Cysteine-Modified Molybdenum Disulfide." *Polymer Bulletin* 78, no. 3 (2020): 1213–30. <https://doi.org/10.1007/s00289-020-03157-9>.

- [14] Kim, Do Young, Jae-Woo Park, and Dong Yun Lee. "Correlation between the Crosslink Characteristics and Mechanical Properties of Natural Rubber Compound via Accelerators and Reinforcement." *Polymers* 12, no. 9 (2020): 2020. <https://doi.org/10.3390/polym12092020>.
- [15] Mohamad, N., Ab Maulod, H. E., Chuan, S.T., et al. "Processability of Uncalcined Tin Dioxide Reinforced Deproteinized Natural Rubber Nanocomposites." In *Proceedings of Mechanical Engineering Research Day 2022*, no. 2022nd ed. (2022).
- [16] Hayemasae, Nabil, and Hanafi Ismail. "Synergistic Improvement of Mechanical and Magnetic Properties of a New Magnetorheological Elastomer Composites Based on Natural Rubber and Powdered Waste Natural Rubber Glove." *Polimeros-Ciencia E Tecnologia*, no. January (2020). <https://doi.org/10.1590/0104-1428.10719>.
- [17] Swapna, Valiya Parambath, Ranimol Stephen, T. Greeshma, C. Sharan Dev, and M. S. Sreekala. "Mechanical and Swelling Behavior of Green Nanocomposites of Natural Rubber Latex and Tubular Shaped Halloysite Nano Clay." *Polymer Composites* 37, no. 2 (2014): 602–11. <https://doi.org/10.1002/pc.23217>.
- [18] Unnikrishnan, G., and Sabu Thomas. "Diffusion and Transport of Aromatic Hydrocarbons through Natural Rubber." *Polymer* 35, no. 25 (1994): 5504–10. [https://doi.org/10.1016/s0032-3861\(05\)80015-1](https://doi.org/10.1016/s0032-3861(05)80015-1).
- [19] Raja, Pandian Bothi, Kabilashen Readdy Munusamy, Veerasadan Perumal, and Mohamad Nasir Mohamad Ibrahim. "Characterization of Nanomaterial Used in Nanobioremediation." In *Elsevier EBooks*, (2022): 57–83. <https://doi.org/10.1016/b978-0-12-823962-9.00037-4>.
- [20] Pulungan, Ahmad Nasir, Basuki Wirjosentono, Eddiyanto, and Sunit Hendrana. "X-Ray Diffraction and Morphology Studies of Sulfonated Polystyrene and Maleated Natural Rubber Blend with PE-g-MA as Compatibilished." *Proceedings of the 1st International Conference on Chemical Science and Technology Innovation ICOCSTI 1*, no. January (2019): 324–28. <https://doi.org/10.5220/0008935003240328>.
- [21] Venkateshaiah, Abhilash, Rajender Nutenki, and K. Suresh. "X-Ray Diffraction Spectroscopy of Polymer Nanocomposites." In *Elsevier EBooks*, (2016): 410–51. <https://doi.org/10.1016/b978-0-323-40183-8.00014-8>.
- [22] Dang, Zhi-Min, Jinkai Yuan, Sheng-Hong Yao, and Ruijin Liao. "Flexible Nanodielectric Materials with High Permittivity for Power Energy Storage." *Advanced Materials* 25, no. 44 (2013): 6334–65. <https://doi.org/10.1002/adma.201301752>.
- [23] Nandiyanto, Asep Bayu Dani, Rosi Oktiani, and Risti Ragadhita. "How to Read and Interpret FTIR Spectroscopy of Organic Material." *Indonesian Journal of Science and Technology* 4, no. 1 (2019): 97. <https://doi.org/10.17509/ijost.v4i1.15806>.
- [24] Abruzzi, Rafael Colombo, Berenice Anina Dedavid, and Marçal Pires. "Characterization of Tin Dioxide Nanoparticles Synthesized by Oxidation." *Cerâmica* 61, 359 (2015): 328–33. <https://doi.org/10.1590/0366-69132015613591919>.
- [25] Kowalczyk, Dorota, and Monika Pitucha. "Application of FTIR Method for the Assessment of Immobilization of Active Substances in the Matrix of Biomedical Materials." *Materials* 12, no. 18 (2019): 2972. <https://doi.org/10.3390/ma12182972>.
- [26] Spasov, Dmitry D., N. A. Ivanova, Artem S. Pushkarev, I. V. Pushkareva, N. N. Presnyakova, Ratibor G. Chumakov, M. Yu. Presnyakov, S.A. Grigoriev, and V. N. Fateev. "On the Influence of Composition and Structure of Carbon-Supported Pt-SnO₂ Hetero-Clusters onto Their Electrocatalytic Activity and Durability in PEMFC." *Catalysts* 9, no. 10 (2019): 803. <https://doi.org/10.3390/catal9100803>.
- [27] Ural, Nazile. "The Significance of Scanning Electron Microscopy (SEM) Analysis on the Microstructure of Improved Clay: An Overview." *Open Geosciences* 13, no. 1 (2021): 197–218. <https://doi.org/10.1515/geo-2020-0145>.
- [28] Rani, Manviri, None Keshu, and Uma Shanker. "Green Nanomaterials: An Overview." In *Elsevier EBooks*, (2022): 43–80. <https://doi.org/10.1016/b978-0-12-823137-1.00026-9>.
- [29] Ghazali, Suriati, M. Mariatti, and Azizan Aziz. "Effects of Filler Shape and Size on the Properties of Silver Filled Epoxy Composite for Electronic Applications." *Journal of Materials Science: Materials in Electronics* 22, no. 1 (2010): 56–63. <https://doi.org/10.1007/s10854-010-0082-2>.
- [30] Suhandani, M. ., Puspitasari, P. ., & Abd Razak, J. "Impact, Hardness and Fracture Morphology of Aluminium Alloy (Al-Si) filled Cobalt Oxide Nanoparticles at Various Stir Casting Temperatures." *Malaysian Journal on Composites Science & Manufacturing* 5, no. 1 (2021): 11–20. <https://doi.org/10.37934/mjcs.5.1.1120>
- [31] Mohamad, N., Muchtar, A., Ghazali, M.J., Dahlan, H.M., Azhari, C.H. "Epoxidised Natural Rubber - Alumina Nanoparticle Composites (ENRAN): Effect of Filler Loading on the Tensile Properties." *Solid State Science and Technology* 17, 2 (2009): 133-143.
- [32] Abd Ghani, A.A., Mohamad, N., Abd Razak, J., Ahsan, Q., Siang Yee, C., Ani, M.A., Ming Teng, M., & Ul-Hamid, A. "Optimization of Hot Press Parameters to Maximize the Physical and Mechanical Properties of Natural Rubber Composites for Elastomeric Mount." *Malaysian Journal on Composites Science & Manufacturing* 1, no. 1 (2020): 27–37. <https://doi.org/10.37934/mjcs.1.1.2737>